www.sciencemag.org/cgi/content/full/science.1254426/DC1

Supplementary Materials for

Conformational dynamics of single HIV-1 envelope trimers on the surface of native virions

James B. Munro,* Jason Gorman, Xiaochu Ma, Zhou Zhou, James Arthos, Dennis R. Burton, Wayne C. Koff, Joel R. Courter, Amos B. Smith III, Peter D. Kwong, Scott C. Blanchard,* Walther Mothes*

*Corresponding author. E-mail: walther.mothes@yale.edu (W.M.); scb2005@med.cornell.edu (S.C.B.); james.munro@tufts.edu (J.B.M.)

Published 8 October 2014 on *Science* Express
DOI: 10.1126/science.1254426

This PDF file includes

Supplementary Materials

Materials and Methods

Construction and testing of tagged viruses

Peptides were inserted directly into the gp120 domain of full-length pNL4-3 using overlap-extension PCR. Tagged viruses were evaluated based on four criteria. First, infectivity of viruses in which all gp120 domains contain either a single tag, or a pair of tags, should be minimally affected by the peptide insertions (fig. S1). Second, tagged Env proteins were required to be processed normally into gp120 and gp41 and incorporated into virions (fig. S2). Third, recognition of tagged Env by the trimer-specific antibodies PG16 and PGT145 was required to ensure that they maintained their native quaternary structure (*33, 34*) (fig. S3). Finally, fluorescent labeling efficiency of the tagged Env sufficient for imaging had to be achieved.

The infectivity of the modified viruses was determined using a luciferase assay (*45*). Briefly, HEK293 cells (ATCC) were maintained in DMEM (Gibco), supplemented with 10% FBS (Gibco), 100 U/ml penicillin/streptomycin (Gibco), and 2 mM L-glutamine (Gibco). Cells were transfected at 50-75% confluency with tagged or wild-type pNL4-3 and a Gaussia luciferase reporter construct (HIV-1-inGLuc) at a ratio of 6:1. Virus was harvested 24 h post-transfection, concentrated 10-fold by centrifugation for 2 h at 20,000 x g over a 10% sucrose cushion. Virus pellets were resuspended in RPMI medium (Gibco) (with 10% FBS, 100 U/ml penicillin/streptomycin, and 2 mM L-glutamine) and titered on MT4 cells (NIH AIDS Research and Reagents Program), which were growing in the same medium. At 36 h post-infection, the Gaussia luciferase activity in the cell supernatant was measured using the BioLux Gaussia Luciferase Assay Kit (New England Biolabs). In addition, infected cells were stained with PE-conjugated anti-p24 antibody KC57 (Beckman Coulter), and subjected to flow cytometery

analysis on a FACSAria flow cytometer (BD Biosciences), as previously described (*46*) (fig. S15). This indicated that at most an MOI of ~0.15 was reached, ensuring that sub-saturating amounts of virus had been used and that the infectivity was measured in a linear range where RLUs correspond to a MOI between 0.15-0.01.

Peptides were inserted into the pCAGGS HIV-1_{JR-FL} gp160 expression plasmid (provided by James Binley) using overlap-extension PCR at positions homologous to those determined for HIV-1_{NL4-3}. HEK293 cells were transfected with tagged or wild-type HIV-1_{JR-FL} gp160 plasmid, pNL4-3 Δ*env*, and HIV-1-inGLuc. Virus was harvested and concentrated as for HIV-1_{NL4-3}, and used to infect A3.01-CCR5 cells, which stably express CCR5 (provided by Alexandra Trkola). The Gaussia luciferase signal was measured as for HIV-1_{NL4-3}. Parallel flow cytometry analysis indicated an MOI of ~0.01.

For both HIV-1 strains, neutralization assays were performed by incubating the concentrated virus with varying concentrations of ligands for 60 min at 37°C prior to infection of the respective target cells. The Gaussia luciferase signal was then measured as for the normal infectivity assays.

The application of smFRET to HIV-1 Env depends on the introduction of enzymatic labeling peptides. In principal, this experimental approach could affect the relative occupancy of the FRET states. However, only a 2-fold effect on infectivity was observed when 100%-tagged Envs containing both labeling peptides were examined (fig. S1). Several lines of evidence lend support to our contention that the tagged viruses closely reflect the behaviors of native Env. First, the 100% V1-Q3/V4-A1-tagged Env is neutralized by the trimer-specific antibodies PG16 and PGT145 to an equivalent extent as observed for wild-type Env (fig. S3A, B). This finding strongly argues that the fully tagged and labeled trimer exhibits native structural, dynamic and

functional properties. This is the tagged Env construct used for the majority of our experiments. The V1-Q3/V5-A1-tagged NL4-3 virus exhibits a somewhat reduced sensitivity to neutralization by PG16 and PGT145 (fig. S3C, D), which could impact the relative occupancies of the FRET states. However, its role in this study is to test if the three FRET states can also be observed from a different structural perspective, rather than to precisely compare the relative occupancies of the FRET states. Second, while minor changes in infectivity can be seen for 100%-tagged viruses (e.g. containing three dually tagged gp120 molecules per Env trimer), all experiments are performed on virus containing a single, dually tagged gp120 molecule embedded within an otherwise wild-type Env trimer. These dually tagged HIV-1_{JR-FL} and HIV-1_{NL4-3} Env molecules reproducibly respond to various ligands including sCD4, antibodies and small-molecule inhibitors in a manner consistent with a large body of virological data. In particular, the response to 17b seen for HIV-1_{NL4-3} by smFRET, and the lack thereof for HIV-1_{JR-FL}, corresponds well with neutralization data (Fig 3C, D). Our ability to succeed with this enzymatic labeling strategy is likely due to the natural variability and known tolerance of these variable loops to accommodate large epitopes (*47-50*).

Fluorophores

smFRET experiments were conducted with Cy3B and Cy5(4S)COT fluorophores, unless otherwise noted. Cy5(4S)COT is a novel intramolecularly photostabilized derivative of the conventional Cy5 fluorophore, to which the triplet state quencher cyclooctotetraene (COT) was linked to increase the effective brightness (photons detected per imaging frame) and total lifetime of the fluorescence (fig. S5) (*22*). Additional sulfonate groups (4S) were added to the

indole moeities of Cy5 to increase aqueous solubility and to minimize non-specific fluorophore binding to membranes.

Purification and labeling of tagged viruses

The tagged HIV-1_{NL4-3} Envs (V1-Q3/V4-A1, and V1-Q3/V5-A1) were subcloned from pNL4-3 into a pNL4-3 construct lacking reverse transcriptase (pNL4-3 Δ*RT*). To generate HIV-1_{NL4-3} particles carrying only a single fluorescently labeled gp120 molecule on the surface of the HIV-1 virus, pNL4-3 Δ*RT* encoding wild-type Env was co-transfected into HEK293 cells at a ratio of 40:1 over the pNL4-3 Δ*RT* plasmid containing the dually-tagged Env. Cell maintenance and transfection was performed as described for infectivity measurements. In the case of HIV-1_{JR-FL}, a 40:1 ratio of wild-type gp160 plasmid to dually-tagged gp160 plasmid was co-transfected along with pNL4-3 Δ*env* Δ*RT*. In both cases, virus was harvested 24 h post-transfection and concentrated by centrifugation for 2 hours at 20,000 x g. Virus pellets were resuspended in Labeling Buffer (50 mM HEPES pH7.5, 10 mM $MgCl_2$, 10 mM $CaCl_2$).

All fluorophore-coenzyme A conjugates were formed by coupling a fluorophore-maleimide to coenzyme A (CoA) (Sigma), followed by purification by reverse-phase high-pressure liquid chromatography as previously described (*51*). The AcpS labeling enzyme was expressed and purified from *E. coli*, as previously described (*51*). The resuspended HIV-1_{NL4-3} and HIV-1_{JR-FL} viruses containing the V1-Q3 and V4-A1 peptide insertions were labeled by incubation with 0.5 μM Cy3B-cadaverine, 0.5 μM Cy5(4S)COT-CoA, 0.65 μM transglutaminase (*20*) (Sigma), and 5 μM AcpS (*19*) for 3 h (HIV-1_{NL4-3}) or overnight (HIV-1_{JR-FL}) at room temperature (fig. S5). The Q3 and A1 peptides were labeled at approximately 40% and 55% efficiency, respectively (see following section on labeling efficiency). Following the

labeling reaction, DSPE-$PEG_{2,000}$-biotin (Avanti) was added to a final concentration of 6 μM (0.02 mg/ml), and the mixture was incubated for an additional 30 min at room temperature. The labeled virus was then purified away from unbound dye and lipid by ultracentrifugation for 1 h at 150,000x g over a 6-18% Optiprep (Sigma) gradient in 50 mM Tris pH 7.4, 100 mM NaCl. The gradients were fractionated, and the fractions containing virus were identified by p24 Western blot analysis. Virus was stored at -80°C until use in smFRET experiments.

Determination of fluorescent labeling efficiency and stoichiometry

The number of donor and acceptor fluorophores per virus was determined by surface-immobilizing fluorescently labeled virions, and imaging under direct excitation of both fluorophores (532-nm and 639-nm excitation) with TIRF microscopy (see following section on smFRET imaging). The number of photobleaching events per virion, for each fluorophore (indicative of the number of fluorophore molecules present on each virus) was then quantified. Cessation of 639-nm excitation then allowed for determination of the number of virions with a single FRET pair, defined as a single donor and a single acceptor fluorophore generating a FRET signal. Of the virions visible under direct excitation of the donor (532 nm only), approximately 23% displayed a single FRET pair. The total number of surface-bound virions, including both labeled and unlabeled virions, was then determined through introduction of an AlexaFluor 488-labeled 2G12 antibody. Unbound antibody was removed by buffer exchange, and surface-immobilized virions were imaged with a 473-nm laser to excite AlexaFluor 488. The number of AlexaFluor 488 puncta were then quantified. These measurements indicated that approximately 39% of the total surface-bound virions contained a single donor fluorophore, 41% contained a single acceptor fluorophore, and 12% contained a single FRET pair (fig. S6).

The extent of non-specific labeling, resulting from incorporation of the fluorophore into the viral membrane, was determined by subjecting untagged virions to labeling and imaging protocols that were identical to those used for the tagged virus. These experiments indicated that approximately 8% and 4% of the observed donor and acceptor fluorescent puncta, respectively, are due to non-specific incorporation of the fluorophores into the viral membrane (fig. S6). The lower level of nonspecific acceptor labeling is likely due to the additional charged sulfonate groups present on the Cy5(4S)COT fluorophore, as compared to Cy3B (fig. S5).

These experimental results were compared to the results of a Monte Carlo simulation in which the number of dually-tagged gp120 domains per virus for 10,000 virions was determined from a binomial distribution, assuming 15 Env trimers per virion, and a 1:40 ratio of dually-tagged:untagged domains. This procedure predicts that approximately 32% of virions remain untagged, 37% contain a single dually tagged gp120 domain, and 31% contain more than one dually tagged domain. The labeling with donor and acceptor fluorophores was similarly simulated using the experimentally observed labeling efficiencies of 40% and 55%, respectively. This analysis also predicts that approximately 24% of the virions would contain a single donor fluorophore, 33% would contain a single acceptor fluorophore, and 11% would contain a single FRET pair. These Monte Carlo simulations also predict that approximately 2% of the virions would contain a non-FRET pair of fluorophores, defined as a single donor and a single acceptor on different gp120 domains. In approximately 5% of this subpopulation both fluorophores would be located on the same trimer. Thus, approximately 0.1% (5% of 2%) of the observed smFRET trajectories may arise from FRET between fluorophores on neighboring gp120 domains in the same Env trimer. The results of this analysis are displayed in fig. S6. The relatively small discrepancy between the experimentally observed stoichiometries and those predicted by

simulation are largely accounted for by non-specific incorporation of fluorophores into the viral membrane, which was not considered in the simulation.

smFRET imaging

Fluorescently labeled virus, containing DSPE-$PEG_{2,000}$-biotin in the viral membrane was immobilized on polyethylene glycol (PEG)-passivated, streptavidin-coated quartz microfluidic devices and imaged at room temperature on a wide-field prism-based TIRF instrument constructed on a Nikon TE2000 inverted microscope body. All smFRET data were acquired using Metamorph software (Molecular Devices). The donor fluorophore was excited with a Ventus 532 nm laser (Laser Quantum). Donor and acceptor fluorescence were collected through a 1.27-NA 60X water-immersion objective (Nikon), optically separated using a 650DCXR dichroic filter (Chroma), and imaged onto Evolve 512 EMCCD arrays (Photometrics). Movies of surface-immobilized viruses were recorded at 25 frames/s for 40 s. All smFRET imaging experiments were performed in buffer containing 50 mM Tris pH7.5, 100 mM NaCl, and a cocktail of triplet-state quenchers (*52*). Also included in the imaging buffer were 2 mM protocatechuic acid, and 8 nM protocatechuate 3,4-deoxygenase to remove molecular oxygen (*53*).

Where indicated, labeled HIV-1 was preincubated with 5 μM $sCD4_{D1D2}$ (0.1 mg/ml) for 60 minutes at room temperature prior to surface immobilization and imaging. Likewise, labeled HIV-1 was incubated with 2 μM 17b Fab (0.1 mg/ml), 0.7 μM antibody (VRC01, PG16, PGT128, PGT145, or 2G12) (0.1 mg/ml), or 100 μM inhibitor (JRC-II-191 or BMS-626529) for 60 minutes (or as indicated) at room temperature prior to imaging. In the case of experiments

involving both $sCD4_{D1D2}$ and 17b Fab, 2 μM 17b Fab was added to the surface-immobilized $sCD4_{D1D2}$-bound virus and similarly incubated.

Analysis of smFRET data

Processing and analysis of fluorescence and smFRET trajectories were carried out using custom-designed Matlab (Mathworks) software. Fluorescence trajectories were extracted from the movies. The background signal was identified following the photobleaching event, and subtracted from the fluorescence trajectories. The background-subtracted fluorescence trajectories were used to calculate the apparent FRET efficiency according to $FRET_{app} = I_A/(\gamma I_D+I_A)$, where I_A and I_D are the intensities of acceptor and donor fluorescence, respectively, and γ is the empirically determined ratio of detection efficiencies on the acceptor and donor channels. The spectral bleed-through of donor fluorescence onto the acceptor channel was determined to be 7.5%. The bleed-through of acceptor fluorescence onto the donor channel was determined to be 15.5%. These values were used to correct the observed FRET efficiency according to $FRET = (FRET_{app} - \alpha)/(1 - \beta - \alpha)$, where $\alpha = 7.5\%$ and $\beta = 15.5\%$. All corrected smFRET trajectories were then subjected to an algorithm that excludes those carrying only a single fluorophore, aggregated or overlapping virus particles exhibiting multiple fluorophores, as well as those that lived less than approximately 5 s. Finally, all trajectories displaying anti-correlated changes in donor and acceptor fluorescence intensities, which are indicative of transitions in FRET efficiency were selected and analysed. Trajectories were compiled into population FRET histograms, and fit to the sum of three Gaussian distributions using a least-squares fitting algorithm in Matlab. smFRET trajectories were fit to a 3-state hidden Markov

model using a segmental *k*-means algorithm (*27*). The dwells identified in each FRET state were used to construct TDPs (*54*).

Supplementary Figures:

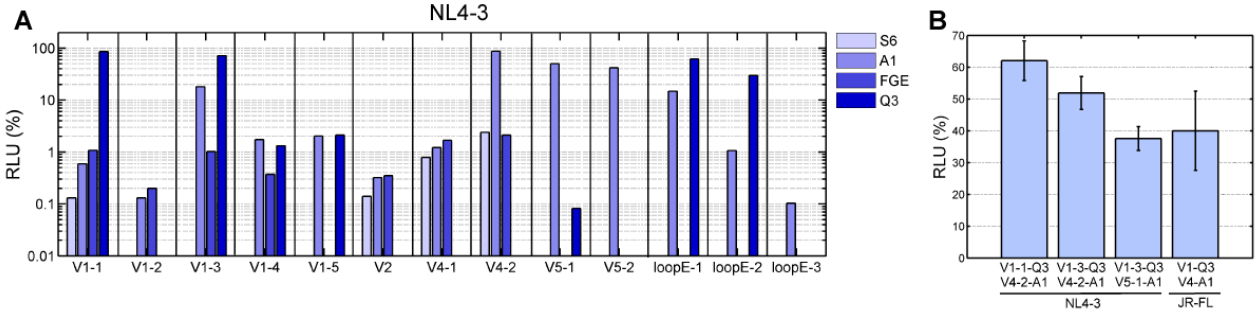

Figure S1 | Infectivity of HIV-1 viruses containing peptides for labeling within variable loops of gp120. (**A**) Four different peptides, corresponding to four orthogonal enzymatic labeling strategies, were inserted into various positions within variable loops V1, V2, V4 and V5, and loop E of the gp120 domain of Env of full-length HIV-1_{NL4-3}. The peptides considered are denoted S6 (GDSLSWLLRLLN) (*19*), A1 (GDSLDMLEWSLM) (*19*), FGE (LCTPSR) (*55*), and Q3 (GQQQLG) (*20*). The infectivity of the viruses containing all gp120 domains bearing a single tag was measured using a Gaussia luciferase assay (*45*), and is displayed as a percentage of wild-type HIV-1_{NL4-3}. (**B**) The peptides inserted into V1 were each combined with the well-tolerated A1 insertion at V4-2 or V5-1, forming three dually tagged viral constructs. The Q3 peptide was inserted into the V1 loop of HIV-1_{JR-FL} Env at a position homologous to V1-3 in HIV-1_{NL4-3}. Likewise, the A1 peptide was inserted into the V4 loop of HIV-1_{JR-FL} Env at a position homologous to V4-2 in HIV-1_{NL4-3}. The infectivity of HIV-1_{NL4-3} and HIV-1_{JR-FL} viruses containing all gp120 domains bearing two tags were determined as in (A). The data are presented as the average of three independent measurements. The data are presented as the mean ± the standard error determined from three independent measurements. RLU, relative light units.

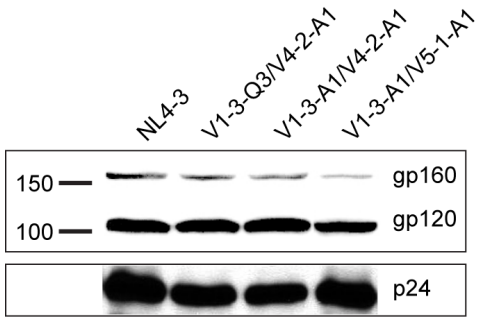

Figure S2 | Tagged Envs are incorporated into virions, and processed into gp120 and gp41. Viral supernatants from cells generating HIV-1_{NL4-3} containing wild-type and dually tagged Env was collected and concentrated by centrifugation. The amount of unprocessed gp160, processed gp120, and p24 antigen in the pellet was visualized by Western blot. The molecular weight (in kDa) marker is indicated at left.

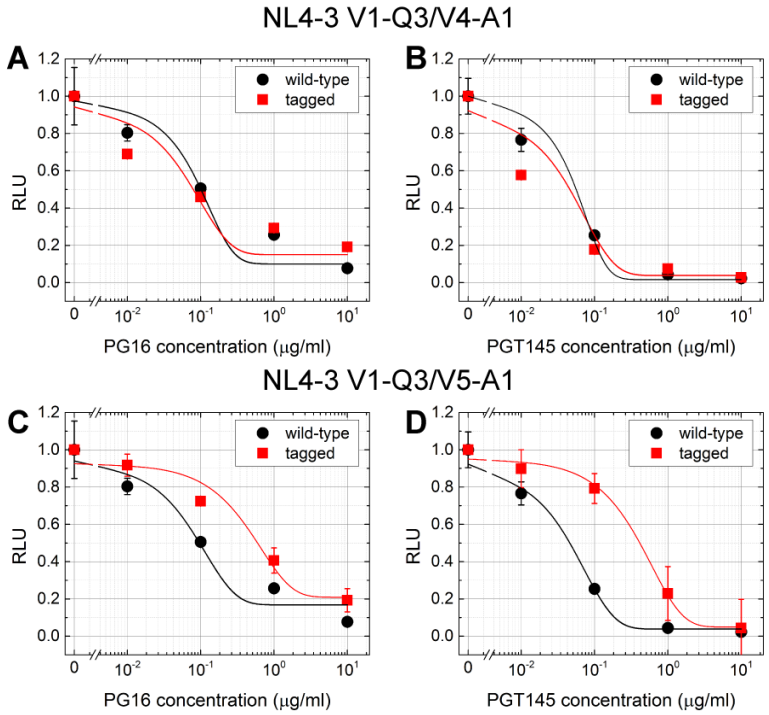

Figure S3 | Dually tagged HIV-1_{NL4-3} viruses are neutralized by trimer-specific antibodies. **(A,B)** Neutralization of the NL4-3 V1-Q3/V4-A1 virus by the PG16 (A) and PGT145 (B) antibodies. The infectivity of virus with tagged Env (red), and wild-type Env (black), in the presence of increasing concentrations of broadly neutralizing antibodies PG16 and PGT145 (*33, 34*). The data are displayed as the infectivity relative to control lacking antibody. (**C,D**) Neutralization of the NL4-3 V1-A1/V5-A1 virus by the PG16 (C) and PGT145 (D) antibodies. The data are presented as the average of three independent measurements. The data are presented as the mean ± the standard error determined from three independent measurements. RLU, relative light units.

V1 loop

```
                                        136
NL4-3           CVKLTPLCVSLKCTDLKND-----TNTNSSSGRMIMEKGEIKNCSFNIS
NL4-3 V1-3-Q3   CVKLTPLCVSLKCTDLKNGQQQLGTNTNSSSGRMIMEKGEIKNCSFNIS
JR-FL           CVKLTPLCVTLNCKDV-N-----ATNTTNDS-EGTMERGEIKNCSFNIT
JR-FL V1-Q3     CVKLTPLCVTLNCKD---GQQQLGTNTTNDS-EGTMERGEIKNCSFNIT
```

V4 loop

```
                                  400
NL4-3           F--NSTW-FNSTW---------------STEGSNNTEGSD
NL4-3 V4-2-A1   F--NSTW-FNSTW---GDSLDMLEWSLMSTEGSNNTEGSD
JR-FL           FYCNSTQLFNSTWNNN-------------TEGSNNTEGNT
JR-FL V4-A1     FYCNSTQLFNSTWNNNGDSLDMLEWSLM-TEGSNNTEGNT
```

V5 loop

```
                                  461
NL4-3           GLLLTRDGGNN------------NNGSEIFRPGGGD
NL4-3 V5-1-A1   GLLLTRDGGNNGDSLDMLEWSLMNNGSEIFRPGGGD
```

Figure S4 | Sites of peptide insertion into variable loops of gp120 of HIV-1. HIV-1_{NL4-3} viruses containing peptide insertions were identified that met the criteria described in Materials and Methods. Homologous insertions were made in HIV-1_{JR-FL} Env. The peptide insertions are indicated in bold, and site of fluorophore ligation is highlighted in red. These sites of insertion are referred to as V1-Q3, V4-A1, and V5-A1 in the text.

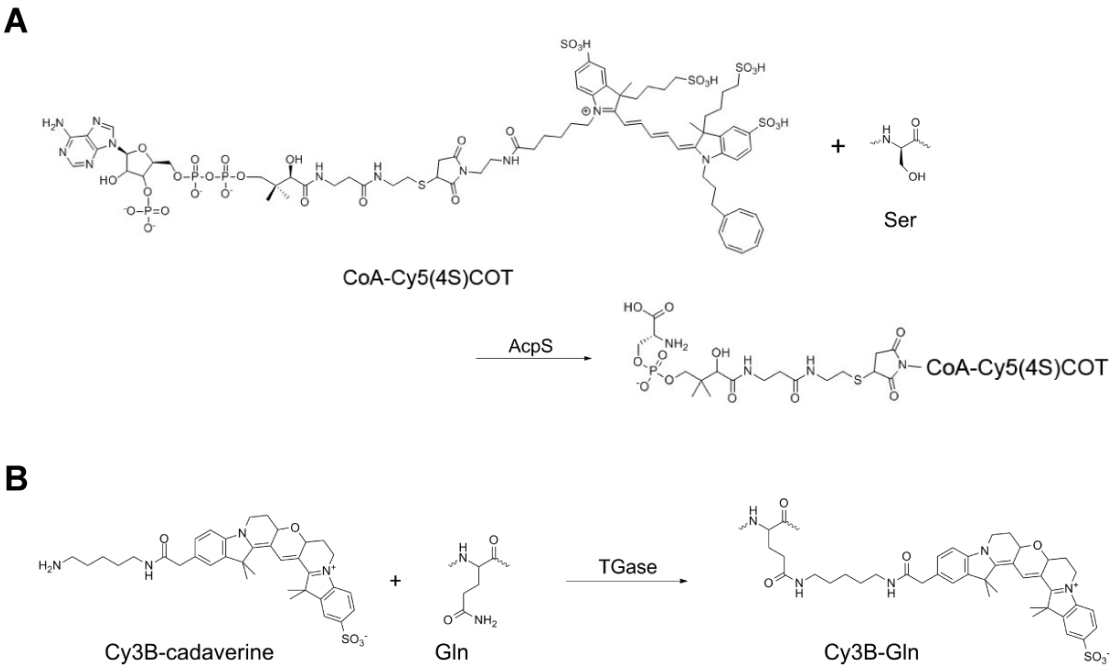

Figure S5 | Enzymatic fluorescent labeling reactions. (**A**) Labeling of the serine residue in the A1 peptide (GDSLDMLEWSLM) through incubation with CoA-Cy5(4S)COT and the AcpS enzyme (*19*). (**B**) The central glutamine residue in the Q3 peptide (GQQQLG) is labeled through incubation with Cy3B-cadaverine and transglutaminase (TGase) (*20*).

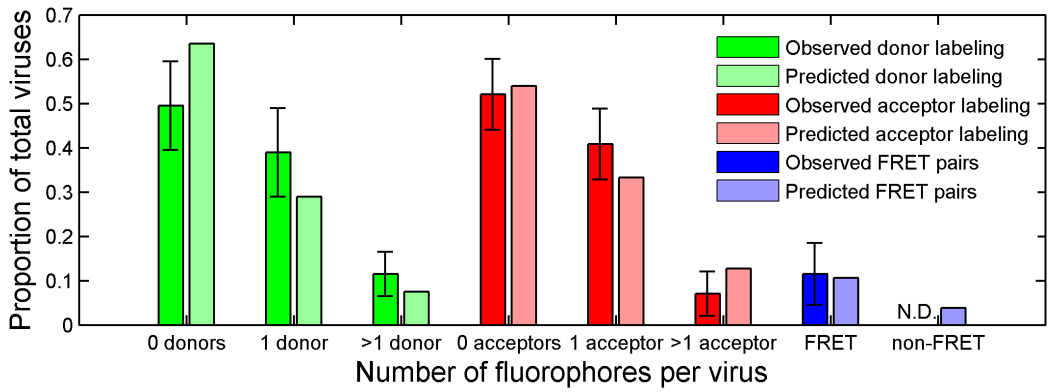

Tagged (V1-Q3/V4-A1)	Experiment (% of total)	MC simulation (% of total)
0 donor molecules	49.5	63.5
1 donor molecule	39.0	29.3
>1 donor molecule	11.5	7.2
0 acceptor molecules	52.1	54.2
1 acceptor molecule	40.8	32.9
>1 acceptor molecule	7.1	12.9
1 FRET pair	11.5	10.9
1 non-FRET pair	ND	2.4
Untagged		
≥1 donor molecule	8.1	ND
≥1 acceptor molecule	4.2	ND
1 FRET pair	0	ND

Figure S6 | Stoichiometry of fluorescent labeling of gp120 on the surface of HIV-1 virions. (**Top**) Graphical and (**Bottom**) numeric comparison of the observed fluorescent labeling stoichiometries to those predicted by Monte-Carlo simulation assuming 15 Env trimers (45 gp120 monomers) per virion, a 1:40 ratio of dually-tagged:untagged gp120, 40% donor labeling efficiency, and 55% acceptor labeling efficiency (see Materials and Methods). For the experimental results, the total number of surface-bound virions (donor-labeled, acceptor-labeled, and unlabeled) was determined through staining with AlexaFluor 488-labeled 2G12 antibody. A FRET pair is defined as one donor and one acceptor on the same gp120 domain. During smFRET imaging experiments, approximately 23% of the visible (donor labeled) molecules displayed FRET. A non-FRET pair is one donor and one acceptor on different gp120 domains. The degree of non-specific binding was quantified by subjecting virions lacking any labeling peptides to the same labeling and imaging protocol as tagged virions. Experimental data is presented as the mean of three independent measurements ± standard error. ND, not determined.

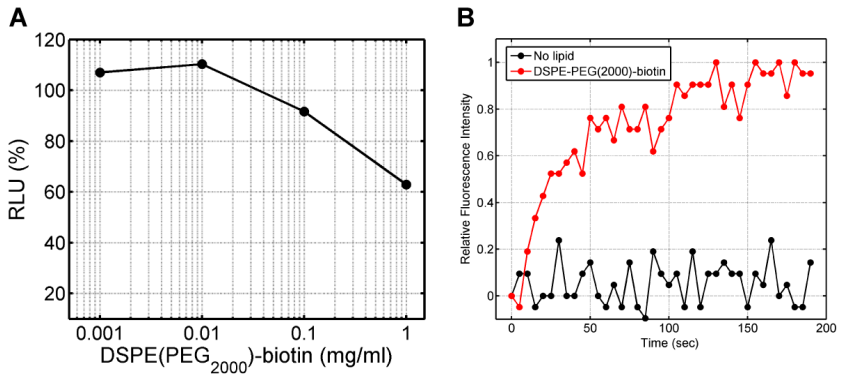

Figure S7 | Surface immobilization of HIV-1 virions. (**A**) The infectivity of HIV-1_{NL4-3} after incubation with varying concentrations of DSPE($PEG_{2,000}$)-biotin (*23*). No loss of infectivity was seen at the concentration used to immobilize virus (0.02 mg/ml). The infectivity is displayed as RLU (relative light units), as a percentage of the no-lipid control. (**B**) The growth of surface-localized fluorescence (red) due to specific immobilization of fluorescent virions on streptavidin-coated quartz microscope slides observed via TIRF microscopy. Without prior incubation with DSPE($PEG_{2,000}$)-biotin no virus bound the surface (black).

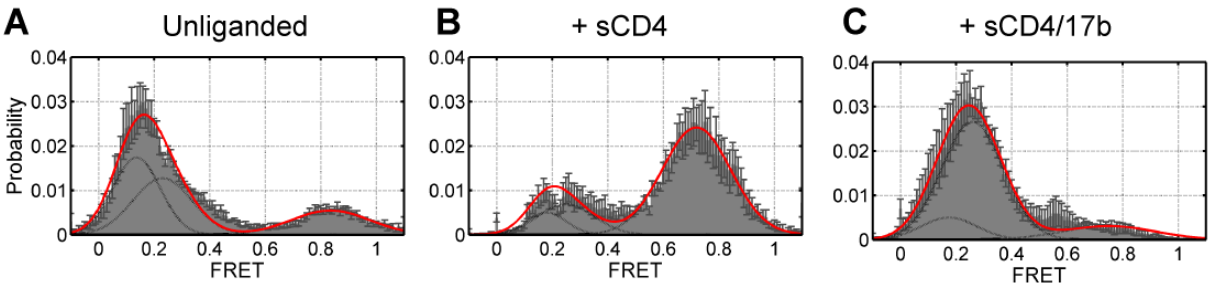

Figure S8 | FRET distribution of HIV-1_{NL4-3} Env containing V1-Q3/V5-A1 peptide insertions. Viruses were labeled with Cy3 at V1-Q3, and AlexaFluor647 at V5-A1. FRET trajectories were compiled into histograms and fit to the sum of three Gaussian distributions with means 0.15, 0.23, and 0.75 (red). FRET histograms obtained (**A**) for the unliganded HIV-1 Env, (**B**) in the presence of $sCD4_{D1D2}$, and (**C**) in the presence of $sCD4_{D1D2}$ and 17b Fab. Each histogram contains 100-150 smFRET trajectories per experiment. Error bars represent the standard errors obtained from three independent populations of FRET traces.

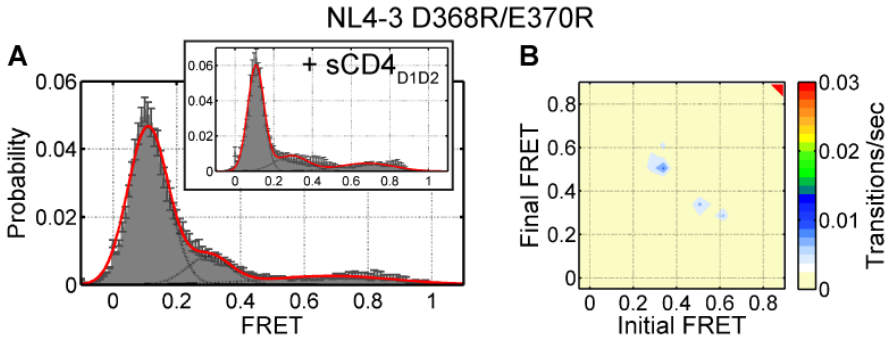

Figure S9 | FRET distribution and dynamics for HIV-1_{NL4-3} with D368R/E370R CD4-binding site mutations. (**A**) FRET histogram (inset, in the presence of $sCD4_{D1D2}$) and (**B**) TDP are displayed as in Fig. 2.

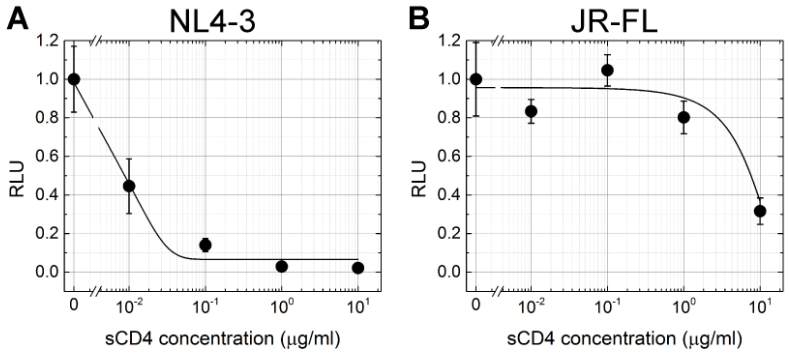

Figure S10 | Neutralization of tagged viruses by $sCD4_{D1D2}$. Neutralization of (**A**) HIV-1_{NL4-3} and (**B**) HIV-1_{JR-FL} by $sCD4_{D1D2}$. The data are displayed as the infectivity relative to control lacking ligand, and are presented as the average of three independent measurements. The data are presented as the mean ± the standard error determined from three independent measurements. RLU, relative light units.

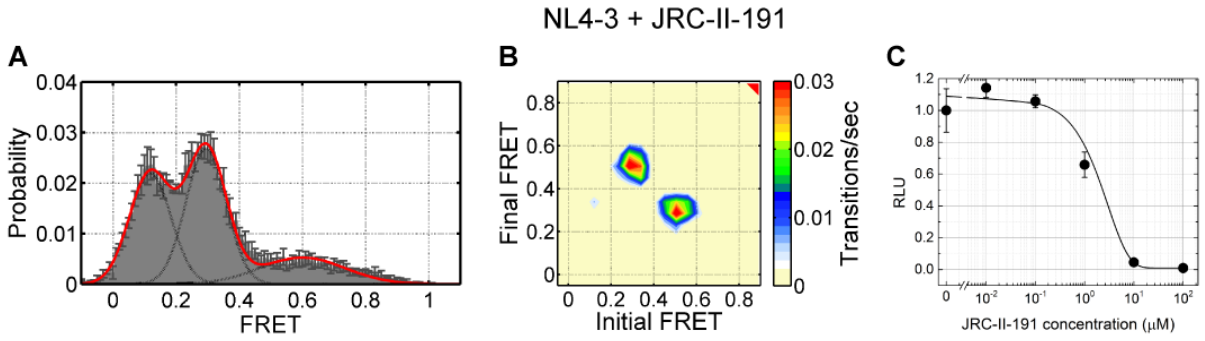

Figure S11 | FRET distribution and dynamics for HIV-1_{NL4-3} in the presence of JRC-II-191. HIV-1_{NL4-3} virus was incubated for 60 min at room temperature with 100 μM JRC-II-191. (**A**) FRET histogram and (**B**) TDP are displayed as in Fig. 2. (**C**) Neutralization of HIV-1_{NL4-3} by JRC-II-191. Data are displayed as in fig. S10.

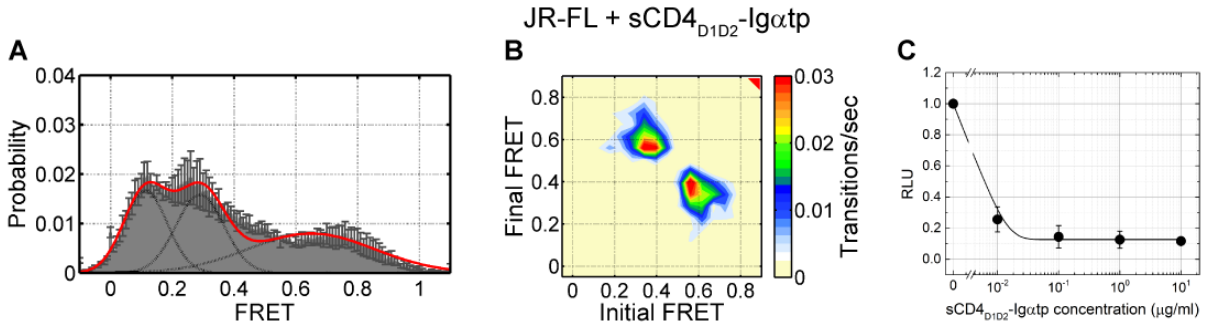

Figure S12 | FRET distribution for HIV-1_{JR-FL} in the presence of $sCD4_{D1D2}$-Igatp. HIV-1_{JR-FL} virus was incubated for 60 min at room temperature with 0.1 mg/ml dodecameric $sCD4_{D1D2}$ prior to imaging (*30*). (**A**) FRET histogram and (**B**) TDP is displayed as in Fig. 2. (**C**) Neutralization of HIV-1_{JR-FL} by $sCD4_{D1D2}$-Igatp. Data are displayed as in fig. S10.

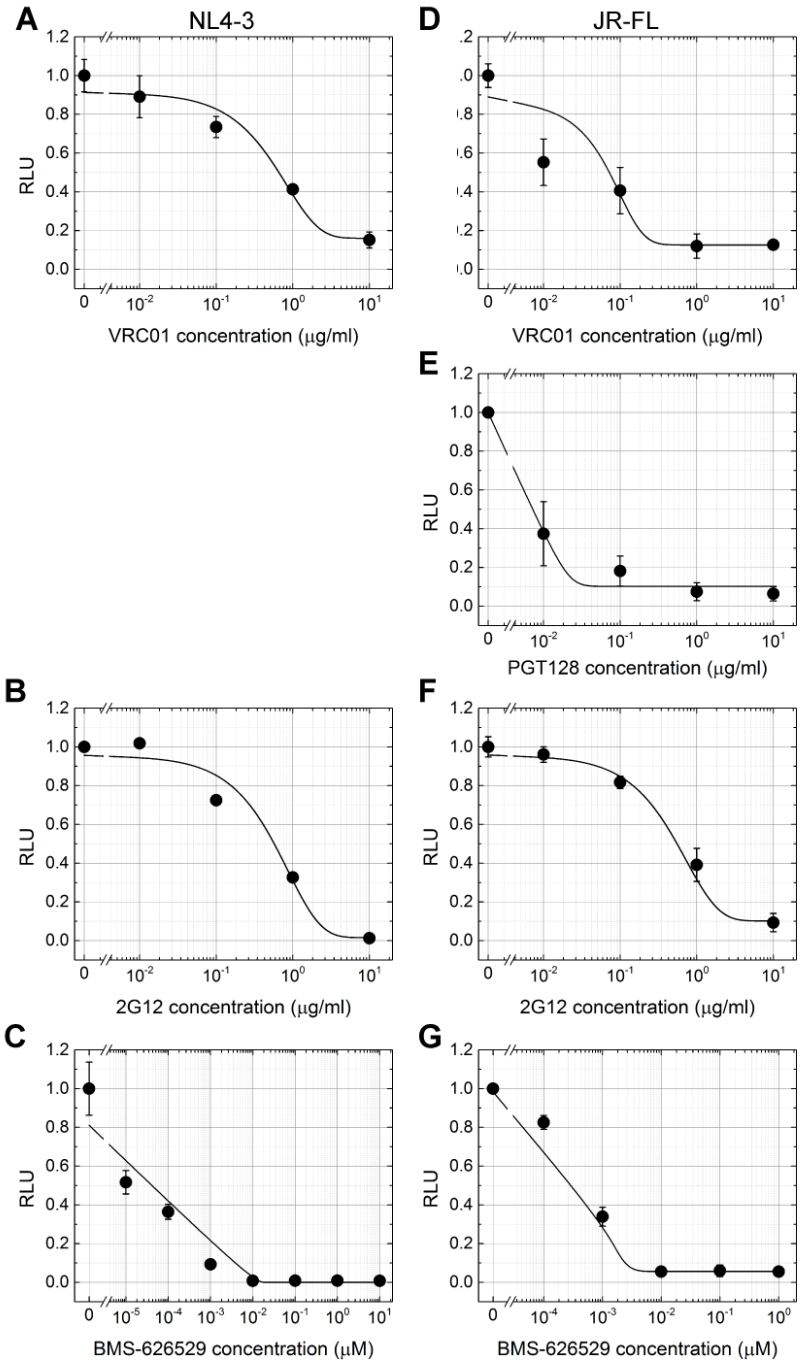

Figure S13 | Neutralization of HIV-1_{NL4-3} and HIV-1_{JR-FL} viruses by broadly neutralizing antibodies and an inhibitor. Neutralization of HIV-1_{NL4-3} by antibodies (**A**) VRC01 and (**B**) 2G12, and (**C**) the small molecule BMS-626529. Neutralization of HIV-1_{JR-FL} by (**D**) VRC01, (**E**) PGT128, (**F**) 2G12, and (**G**) BMS-626529. The data are displayed as in fig. S10.

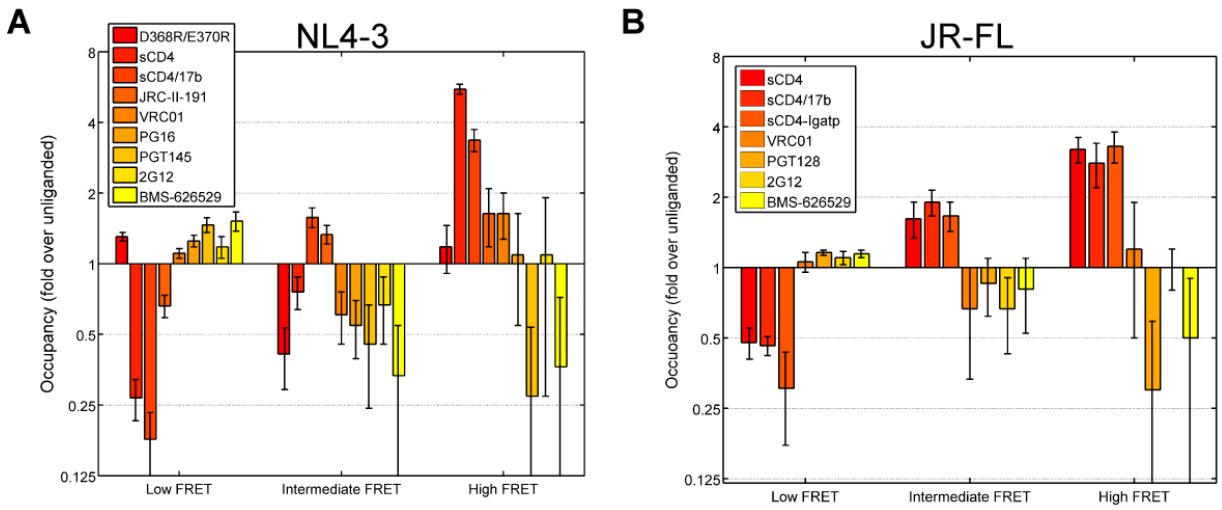

Figure S14 | Changes in the occupancy of the FRET states as a result of ligand binding. Occupancies in the three FRET states were determined by hidden Markov modeling of the individual smFRET trajectories. (**A**) The changes in the occupancy of the low-, intermediate-, and high-FRET states of HIV-1_{NL4-3} Env in response to binding of the indicated ligand. The occupancy is presented as the fold change over that found for the unliganded Env. (**B**) The same data for HIV-1_{JR-FL} Env. The data are presented as the mean ± the standard error determined from three independent groups of smFRET traces.

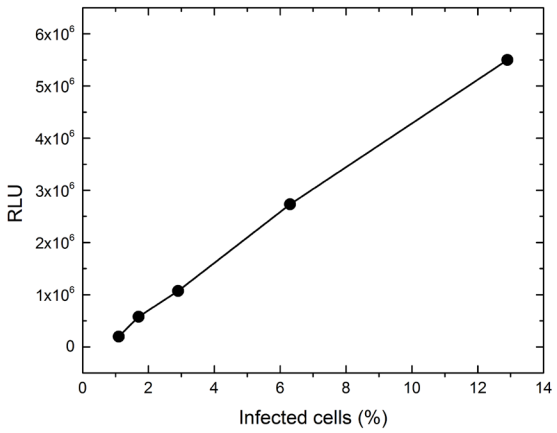

Figure S15 | Flow cytometry analysis of HIV-1_{NL4-3} infection. MT4 cells infected with HIV-1_{NL4-3} were subjected to flow cytometry analysis for p24 positive cells in order to estimate the percentage of cells infected. These data were then correlated with parallel infectivity measurements of relative light units (RLU) using the Gaussia luciferase assay. The infectivity and neutralization data presented throughout involved luminescence values in the 1-2 x 10^6 RLU range, well within the linear response range.

Supplementary Tables:

	Anisotropy (*r*)
Cy5	0.13 ± 0.01
V1-3-Q3(Cy5)	0.18 ± 0.01
V1-3-Q3(Cy5) + sCD4	0.17 ± 0.01
V1-3-Q3(Cy5) + sCD4/17b	0.19 ± 0.02
Cy3B	0.23 ± 0.01
V4-2-A1(Cy3B)	0.22 ± 0.01
V4-2-A1(Cy3B) + sCD4	0.23 ± 0.01
V4-2-A1(Cy3B) + sCD4/17b	0.22 ± 0.02
V5-1-A1(Cy3B)	0.18 ± 0.03
V5-1-A1(Cy3B) + sCD4	0.21 ± 0.02
V5-1-A1(Cy3B) + sCD4/17b	0.19 ± 0.01

Table S1 | Fluorescence anisotropy from Cy5 and Cy3B bound to HIV-1 Env. Due to the inherently short fluorescence lifetimes (~1 ns) of the fluorophores, sufficient tumbling does not occur during occupancy in the excited state to randomize the polarization of the emitted fluorescence. Therefore all anisotropy values are above the optimal value of 0.1. The data are presented as the mean ± the standard error determined from three independent measurements.

HIV-1_{JR-FL}	**Low (0.1)**	**Intermediate (0.3)**	**High (0.65)**
Unliganded	69±6%	21±6%	10±6%
$sCD4_{D1D2}$	33±3%	34±5%	32±6%
$sCD4_{D1D2}$/17b	32±9%	40±5%	28±5%
$sCD4_{D1D2}$-Ig □tp	29±8%	31±8%	40±8%
VRC01	73±4%	14±5%	12±5%
PGT128	80±5%	18±5%	3±2%
2G12	76±3%	14±6%	10±4%
BMS-626529	79±3%	17±7%	4±5%
HIV-1_{NL4-3}	**Low (0.1)**	**Intermediate (0.3)**	**High (0.6)**
Unliganded	56±3%	33±4%	11±3%
D368R/E370R	73±3%	14±5%	13±7%
$sCD4_{D1D2}$	15±3%	25±4%	61±3%
$sCD4_{D1D2}$/17b	10±3%	52±5%	37±4%
JRC-II-191	37±4%	44±4%	18±5%
VRC01	62±3%	20±5%	18±4%
PG16	70±4%	18±5%	12±6%
PGT145	82±6%	15±7%	3±4%
2G12	66±7%	22±7%	12±9%
BMS-626529	85±8%	11±7%	4±9%

Table S2 | Occupancies in each of the three observed FRET states determined through hidden Markov modeling. The data are presented as the mean ± the standard error determined from three independent groups of smFRET traces.

NL4-3				**JR-FL**		
→0.65	0.90	0.89	--	0.81	0.91	--
→0.3	0.10	--	0.38	0.19	--	0.65
→0.1	--	0.11	0.62	--	0.09	0.35
	0.1→	**0.3 →**	**0.65→**	**0.1→**	**0.3 →**	**0.6→**

NL4-3 + sCD4				**JR-FL + sCD4**		
→0.65	0.78	0.89	--	0.89	0.91	--
→0.3	0.22	--	0.76	0.11	--	0.51
→0.1	--	0.11	0.24	--	0.09	0.49
	0.1→	**0.3 →**	**0.65→**	**0.1→**	**0.3 →**	**0.6→**

NL4-3 + sCD4/17b				**JR-FL + sCD4/17b**		
→0.65	0.67	0.91	--	0.96	0.02	--
→0.3	0.33	--	0.85	0.04	--	0.65
→0.1	--	0.09	0.15	--	0.98	0.35
	0.1→	**0.3 →**	**0.65→**	**0.1→**	**0.3 →**	**0.6→**

NL4-3 + JRC-II-191			
→0.65	0.63	0.93	--
→0.3	0.37	--	0.90
→0.1	--	0.07	0.10
	0.1→	**0.3 →**	**0.6→**

Table S3 | Transition probabilities determined through hidden Markov modeling of smFRET trajectories. smFRET trajectories were fit to a three-state hidden Markov model using a segmental *k*-means algorithm (*27*). The transitions between each state were tabulated. The data are presented as the proportion of transitions into each state.

References and Notes

1. S. C. Harrison, Viral membrane fusion. *Nat. Struct. Mol. Biol.* **15**, 690–698 (2008). Medline doi:10.1038/nsmb.1456

2. R. Wyatt, J. Sodroski, The HIV-1 envelope glycoproteins: Fusogens, antigens, and immunogens. *Science* **280**, 1884–1888 (1998). Medline doi:10.1126/science.280.5371.1884

3. R. Pantophlet, D. R. Burton, GP120: Target for neutralizing HIV-1 antibodies. *Annu. Rev. Immunol.* **24**, 739–769 (2006). Medline doi:10.1146/annurev.immunol.24.021605.090557

4. X. Wei, J. M. Decker, S. Wang, H. Hui, J. C. Kappes, X. Wu, J. F. Salazar-Gonzalez, M. G. Salazar, J. M. Kilby, M. S. Saag, N. L. Komarova, M. A. Nowak, B. H. Hahn, P. D. Kwong, G. M. Shaw, Antibody neutralization and escape by HIV-1. *Nature* **422**, 307–312 (2003). Medline doi:10.1038/nature01470

5. R. Wyatt, P. D. Kwong, E. Desjardins, R. W. Sweet, J. Robinson, W. A. Hendrickson, J. G. Sodroski, The antigenic structure of the HIV gp120 envelope glycoprotein. *Nature* **393**, 705–711 (1998). Medline doi:10.1038/31514

6. J.-P. Julien, A. Cupo, D. Sok, R. L. Stanfield, D. Lyumkis, M. C. Deller, P.-J. Klasse, D. R. Burton, R. W. Sanders, J. P. Moore, A. B. Ward, I. A. Wilson, Crystal structure of a soluble cleaved HIV-1 envelope trimer. *Science* **342**, 1477–1483 (2013). Medline doi:10.1126/science.1245625

7. D. Lyumkis, J.-P. Julien, N. de Val, A. Cupo, C. S. Potter, P.-J. Klasse, D. R. Burton, R. W. Sanders, J. P. Moore, B. Carragher, I. A. Wilson, A. B. Ward, Cryo-EM structure of a fully glycosylated soluble cleaved HIV-1 envelope trimer. *Science* **342**, 1484–1490 (2013). Medline doi:10.1126/science.1245627

8. J. Liu, A. Bartesaghi, M. J. Borgnia, G. Sapiro, S. Subramaniam, Molecular architecture of native HIV-1 gp120 trimers. *Nature* **455**, 109–113 (2008). Medline doi:10.1038/nature07159

9. T. A. White, A. Bartesaghi, M. J. Borgnia, J. R. Meyerson, M. J. de la Cruz, J. W. Bess, R. Nandwani, J. A. Hoxie, J. D. Lifson, J. L. Milne, S. Subramaniam, Molecular architectures of trimeric SIV and HIV-1 envelope glycoproteins on intact viruses: Strain-dependent variation in quaternary structure. *PLOS Pathog.* **6**, e1001249 (2010). Medline

10. G. Hu, J. Liu, K. A. Taylor, K. H. Roux, Structural comparison of HIV-1 envelope spikes with and without the V1/V2 loop. *J. Virol.* **85**, 2741–2750 (2011). Medline doi:10.1128/JVI.01612-10

11. P. D. Kwong, R. Wyatt, J. Robinson, R. W. Sweet, J. Sodroski, W. A. Hendrickson, Structure of an HIV gp120 envelope glycoprotein in complex with the CD4 receptor and a neutralizing human antibody. *Nature* **393**, 648–659 (1998). Medline doi:10.1038/31405

12. M. Pancera, S. Majeed, Y. E. Ban, L. Chen, C. C. Huang, L. Kong, Y. D. Kwon, J. Stuckey, T. Zhou, J. E. Robinson, W. R. Schief, J. Sodroski, R. Wyatt, P. D. Kwong, Structure of HIV-1 gp120 with gp41-interactive region reveals layered envelope architecture and basis of conformational mobility. *Proc. Natl. Acad. Sci. U.S.A.* **107**, 1166–1171 (2010). Medline doi:10.1073/pnas.0911004107

13. E. E. Tran, M. J. Borgnia, O. Kuybeda, D. M. Schauder, A. Bartesaghi, G. A. Frank, G. Sapiro, J. L. Milne, S. Subramaniam, Structural mechanism of trimeric HIV-1 envelope glycoprotein activation. *PLOS Pathog.* **8**, e1002797 (2012). Medline doi:10.1371/journal.ppat.1002797

14. Y. Mao, L. Wang, C. Gu, A. Herschhorn, S. H. Xiang, H. Haim, X. Yang, J. Sodroski, Subunit organization of the membrane-bound HIV-1 envelope glycoprotein trimer. *Nat. Struct. Mol. Biol.* **19**, 893–899 (2012). Medline doi:10.1038/nsmb.2351

15. A. Harris, M. J. Borgnia, D. Shi, A. Bartesaghi, H. He, R. Pejchal, Y. K. Kang, R. Depetris, A. J. Marozsan, R. W. Sanders, P.-J. Klasse, J. L. Milne, I. A. Wilson, W. C. Olson, J. P. Moore, S. Subramaniam, Trimeric HIV-1 glycoprotein gp140 immunogens and native HIV-1 envelope glycoproteins display the same closed and open quaternary molecular architectures. *Proc. Natl. Acad. Sci. U.S.A.* **108**, 11440–11445 (2011). Medline doi:10.1073/pnas.1101414108

16. C. G. Moscoso, Y. Sun, S. Poon, L. Xing, E. Kan, L. Martin, D. Green, F. Lin, A. G. Vahlne, S. Barnett, I. Srivastava, R. H. Cheng, Quaternary structures of HIV Env immunogen exhibit conformational vicissitudes and interface diminution elicited by ligand binding. *Proc. Natl. Acad. Sci. U.S.A.* **108**, 6091–6096 (2011). Medline doi:10.1073/pnas.1016113108

17. S. R. Wu, R. Löving, B. Lindqvist, H. Hebert, P. J. Koeck, M. Sjöberg, H. Garoff, Single-particle cryoelectron microscopy analysis reveals the HIV-1 spike as a tripod structure. *Proc. Natl. Acad. Sci. U.S.A.* **107**, 18844–18849 (2010). Medline doi:10.1073/pnas.1007227107

18. R. Roy, S. Hohng, T. Ha, A practical guide to single-molecule FRET. *Nat. Methods* **5**, 507–516 (2008). Medline doi:10.1038/nmeth.1208

19. Z. Zhou, P. Cironi, A. J. Lin, Y. Xu, S. Hrvatin, D. E. Golan, P. A. Silver, C. T. Walsh, J. Yin, Genetically encoded short peptide tags for orthogonal protein labeling by Sfp and AcpS phosphopantetheinyl transferases. *ACS Chem. Biol.* **2**, 337–346 (2007). Medline doi:10.1021/cb700054k

20. C. W. Lin, A. Y. Ting, Transglutaminase-catalyzed site-specific conjugation of small-molecule probes to proteins in vitro and on the surface of living cells. *J. Am. Chem. Soc.* **128**, 4542–4543 (2006). Medline doi:10.1021/ja0604111

21. Materials and Methods are available as supplementary materials on *Science* Online.

22. Q. Zheng, M. F. Juette, S. Jockusch, M. R. Wasserman, Z. Zhou, R. B. Altman, S. C. Blanchard, Ultra-stable organic fluorophores for single-molecule research. *Chem. Soc. Rev.* **43**, 1044–1056 (2014). Medline doi:10.1039/c3cs60237k

23. N. G. Mukherjee, L. A. Lyon, J. M. Le Doux, Rapid modification of retroviruses using lipid conjugates. *Nanotechnology* **20**, 065103 (2009). Medline doi:10.1088/0957-4484/20/6/065103

24. K. Henzler-Wildman, D. Kern, Dynamic personalities of proteins. *Nature* **450**, 964–972 (2007). Medline doi:10.1038/nature06522

25. P. D. Kwong, M. L. Doyle, D. J. Casper, C. Cicala, S. A. Leavitt, S. Majeed, T. D. Steenbeke, M. Venturi, I. Chaiken, M. Fung, H. Katinger, P. W. Parren, J. Robinson, D. Van Ryk, L. Wang, D. R. Burton, E. Freire, R. Wyatt, J. Sodroski, W. A. Hendrickson, J. Arthos, HIV-1 evades antibody-mediated neutralization through conformational masking of receptor-binding sites. *Nature* **420**, 678–682 (2002). Medline doi:10.1038/nature01188

26. U. Olshevsky, E. Helseth, C. Furman, J. Li, W. Haseltine, J. Sodroski, Identification of individual human immunodeficiency virus type 1 gp120 amino acids important for CD4 receptor binding. *J. Virol.* **64**, 5701–5707 (1990). Medline

27. F. Qin, Restoration of single-channel currents using the segmental k-means method based on hidden Markov modeling. *Biophys. J.* **86**, 1488–1501 (2004). Medline doi:10.1016/S0006-3495(04)74217-4

28. H. Haim, Z. Si, N. Madani, L. Wang, J. R. Courter, A. Princiotto, A. Kassa, M. DeGrace, K. McGee-Estrada, M. Mefford, D. Gabuzda, A. B. Smith 3rd, J. Sodroski, Soluble CD4 and CD4-mimetic compounds inhibit HIV-1 infection by induction of a short-lived activated state. *PLOS Pathog.* **5**, e1000360 (2009). Medline doi:10.1371/journal.ppat.1000360

29. N. Sullivan, Y. Sun, Q. Sattentau, M. Thali, D. Wu, G. Denisova, J. Gershoni, J. Robinson, J. Moore, J. Sodroski, CD4-Induced conformational changes in the human immunodeficiency virus type 1 gp120 glycoprotein: Consequences for virus entry and neutralization. *J. Virol.* **72**, 4694–4703 (1998). Medline

30. J. Arthos, C. Cicala, T. D. Steenbeke, T.-W. Chun, C. Dela Cruz, D. B. Hanback, P. Khazanie, D. Nam, P. Schuck, S. M. Selig, D. Van Ryk, M. A. Chaikin, A. S. Fauci, Biochemical and biological characterization of a dodecameric CD4-Ig fusion protein: Implications for therapeutic and vaccine strategies. *J. Biol. Chem.* **277**, 11456–11464 (2002). Medline doi:10.1074/jbc.M111191200

31. A. L. DeVico, CD4-induced epitopes in the HIV envelope glycoprotein, gp120. *Curr. HIV Res.* **5**, 561–571 (2007). Medline doi:10.2174/157016207782418560

32. T. Zhou, I. Georgiev, X. Wu, Z.-Y. Yang, K. Dai, A. Finzi, Y. D. Kwon, J. F. Scheid, W. Shi, L. Xu, Y. Yang, J. Zhu, M. C. Nussenzweig, J. Sodroski, L. Shapiro, G. J. Nabel, J. R. Mascola, P. D. Kwong, Structural basis for broad and potent neutralization of HIV-1 by antibody VRC01. *Science* **329**, 811–817 (2010). Medline doi:10.1126/science.1192819

33. L. M. Walker, S. K. Phogat, P. Y. Chan-Hui, D. Wagner, P. Phung, J. L. Goss, T. Wrin, M. D. Simek, S. Fling, J. L. Mitcham, J. K. Lehrman, F. H. Priddy, O. A. Olsen, S. M. Frey, P. W. Hammond, S. Kaminsky, T. Zamb, M. Moyle, W. C. Koff, P. Poignard, D. R. Burton; Protocol G Principal Investigators, Broad and potent neutralizing antibodies from an African donor reveal a new HIV-1 vaccine target. *Science* **326**, 285–289 (2009). Medline doi:10.1126/science.1178746

34. L. M. Walker, M. Huber, K. J. Doores, E. Falkowska, R. Pejchal, J.-P. Julien, S.-K. Wang, A. Ramos, P.-Y. Chan-Hui, M. Moyle, J. L. Mitcham, P. W. Hammond, O. A. Olsen, P. Phung, S. Fling, C.-H. Wong, S. Phogat, T. Wrin, M. D. Simek, W. C. Koff, I. A. Wilson, D. R. Burton, P. Poignard; Protocol G Principal Investigators, Broad neutralization coverage of HIV by multiple highly potent antibodies. *Nature* **477**, 466–470 (2011). Medline doi:10.1038/nature10373

35. M. Pancera, S. Shahzad-Ul-Hussan, N. A. Doria-Rose, J. S. McLellan, R. T. Bailer, K. Dai, S. Loesgen, M. K. Louder, R. P. Staupe, Y. Yang, B. Zhang, R. Parks, J. Eudailey, K. E. Lloyd, J. Blinn, S. M. Alam, B. F. Haynes, M. N. Amin, L. X. Wang, D. R. Burton, W. C. Koff, G. J. Nabel, J. R. Mascola, C. A. Bewley, P. D. Kwong, Structural basis for diverse N-glycan recognition by HIV-1-neutralizing V1-V2-directed antibody PG16. *Nat. Struct. Mol. Biol.* **20**, 804–813 (2013). Medline doi:10.1038/nsmb.2600

36. J.-P. Julien, J. H. Lee, A. Cupo, C. D. Murin, R. Derking, S. Hoffenberg, M. J. Caulfield, C. R. King, A. J. Marozsan, P.-J. Klasse, R. W. Sanders, J. P. Moore, I. A. Wilson, A. B. Ward, Asymmetric recognition of the HIV-1 trimer by broadly neutralizing antibody PG9. *Proc. Natl. Acad. Sci. U.S.A.* **110**, 4351–4356 (2013). Medline doi:10.1073/pnas.1217537110

37. J.-P. Julien, D. Sok, R. Khayat, J. H. Lee, K. J. Doores, L. M. Walker, A. Ramos, D. C. Diwanji, R. Pejchal, A. Cupo, U. Katpally, R. S. Depetris, R. L. Stanfield, R. McBride, A. J. Marozsan, J. C. Paulson, R. W. Sanders, J. P. Moore, D. R. Burton, P. Poignard, A. B. Ward, I. A. Wilson, Broadly neutralizing antibody PGT121 allosterically modulates CD4 binding via recognition of the HIV-1 gp120 V3 base and multiple surrounding glycans. *PLOS Pathog.* **9**, e1003342 (2013). Medline doi:10.1371/journal.ppat.1003342

38. P. D. Kwong, J. R. Mascola, G. J. Nabel, Broadly neutralizing antibodies and the search for an HIV-1 vaccine: The end of the beginning. *Nat. Rev. Immunol.* **13**, 693–701 (2013). Medline doi:10.1038/nri3516

39. Z. Li, N. Zhou, Y. Sun, N. Ray, M. Lataillade, G. J. Hanna, M. Krystal, Activity of the HIV-1 attachment inhibitor BMS-626529, the active component of the prodrug BMS-663068, against CD4-independent viruses and HIV-1 envelopes resistant to other entry inhibitors. *Antimicrob. Agents Chemother.* **57**, 4172–4180 (2013). Medline doi:10.1128/AAC.00513-13

40. J. B. Munro, K. Y. Sanbonmatsu, C. M. Spahn, S. C. Blanchard, Navigating the ribosome's metastable energy landscape. *Trends Biochem. Sci.* **34**, 390–400 (2009). Medline doi:10.1016/j.tibs.2009.04.004

41. Subsequent to the submission of this manuscript, the structure of a trimeric pre-fusion HIV-1 Env (*42*) was determined in complex with broadly neutralizing antibodies antibodies PGT122 (*34*) and 35O22 (*43*). To determine the conformational state these antibodies captured in the crystal lattice, we measured smFRET on labeled JR-FL virions in the presence of either PGT122, 35O22 or both. These data indicated that PGT122 strongly stabilized the ground state. In contrast 35O22 had little effect on Env conformation. HIV-1 Env complexed with both antibodies exhibited slight ground state stabilization.

42. M. Pancera *et al.*, Structure and immune recognition of trimeric prefusion HIV-1 Env. *Nature* 10.1038/nature13808 (2014).

43. J. Huang, B. H. Kang, M. Pancera, J. H. Lee, T. Tong, Y. Feng, I. S. Georgiev, G. Y. Chuang, A. Druz, N. A. Doria-Rose, L. Laub, K. Sliepen, M. J. van Gils, A. T. de la Peña, R. Derking, P.-J. Klasse, S. A. Migueles, R. T. Bailer, M. Alam, P. Pugach, B. F. Haynes, R. T. Wyatt, R. W. Sanders, J. M. Binley, A. B. Ward, J. R. Mascola, P. D. Kwong, M. Connors, Broad and potent HIV-1 neutralization by a human antibody that

binds the gp41-gp120 interface. *Nature* •••, (2014). 10.1038/nature13601 Medline doi:10.1038/nature13601

44. J. S. McLellan, M. Pancera, C. Carrico, J. Gorman, J.-P. Julien, R. Khayat, R. Louder, R. Pejchal, M. Sastry, K. Dai, S. O'Dell, N. Patel, S. Shahzad-ul-Hussan, Y. Yang, B. Zhang, T. Zhou, J. Zhu, J. C. Boyington, G.-Y. Chuang, D. Diwanji, I. Georgiev, Y. D. Kwon, D. Lee, M. K. Louder, S. Moquin, S. D. Schmidt, Z.-Y. Yang, M. Bonsignori, J. A. Crump, S. H. Kapiga, N. E. Sam, B. F. Haynes, D. R. Burton, W. C. Koff, L. M. Walker, S. Phogat, R. Wyatt, J. Orwenyo, L.-X. Wang, J. Arthos, C. A. Bewley, J. R. Mascola, G. J. Nabel, W. R. Schief, A. B. Ward, I. A. Wilson, P. D. Kwong, Structure of HIV-1 gp120 V1/V2 domain with broadly neutralizing antibody PG9. *Nature* **480**, 336–343 (2011). Medline doi:10.1038/nature10696

45. P. Zhong, L. M. Agosto, A. Ilinskaya, B. Dorjbal, R. Truong, D. Derse, P. D. Uchil, G. Heidecker, W. Mothes, Cell-to-cell transmission can overcome multiple donor and target cell barriers imposed on cell-free HIV. *PLOS ONE* **8**, e53138 (2013). Medline doi:10.1371/journal.pone.0053138

46. L. M. Agosto, P. Zhong, J. Munro, W. Mothes, Highly active antiretroviral therapies are effective against HIV-1 cell-to-cell transmission. *PLOS Pathog.* **10**, e1003982 (2014). Medline doi:10.1371/journal.ppat.1003982

47. K. Leung, J. O. Kim, L. Ganesh, J. Kabat, O. Schwartz, G. J. Nabel, HIV-1 assembly: Viral glycoproteins segregate quantally to lipid rafts that associate individually with HIV-1 capsids and virions. *Cell Host Microbe* **3**, 285–292 (2008). Medline doi:10.1016/j.chom.2008.04.004

48. X. Yang, I. Lipchina, S. Cocklin, I. Chaiken, J. Sodroski, Antibody binding is a dominant determinant of the efficiency of human immunodeficiency virus type 1 neutralization. *J. Virol.* **80**, 11404–11408 (2006). Medline doi:10.1128/JVI.01102-06

49. X. Ren, J. Sodroski, X. Yang, An unrelated monoclonal antibody neutralizes human immunodeficiency virus type 1 by binding to an artificial epitope engineered in a functionally neutral region of the viral envelope glycoproteins. *J. Virol.* **79**, 5616–5624 (2005). Medline doi:10.1128/JVI.79.9.5616-5624.2005

50. M. E. Laird, R. C. Desrosiers, Infectivity and neutralization of simian immunodeficiency virus with FLAG epitope insertion in gp120 variable loops. *J. Virol.* **81**, 10838–10848 (2007). Medline doi:10.1128/JVI.00831-07

51. J. Yin, A. J. Lin, D. E. Golan, C. T. Walsh, Site-specific protein labeling by Sfp phosphopantetheinyl transferase. *Nat. Protoc.* **1**, 280–285 (2006). Medline doi:10.1038/nprot.2006.43

52. R. Dave, D. S. Terry, J. B. Munro, S. C. Blanchard, Mitigating unwanted photophysical processes for improved single-molecule fluorescence imaging. *Biophys. J.* **96**, 2371–2381 (2009). Medline doi:10.1016/j.bpj.2008.11.061

53. C. E. Aitken, R. A. Marshall, J. D. Puglisi, An oxygen scavenging system for improvement of dye stability in single-molecule fluorescence experiments. *Biophys. J.* **94**, 1826–1835 (2008). Medline doi:10.1529/biophysj.107.117689

54. S. A. McKinney, C. Joo, T. Ha, Analysis of single-molecule FRET trajectories using hidden Markov modeling. *Biophys. J.* **91**, 1941–1951 (2006). Medline doi:10.1529/biophysj.106.082487

55. P. Wu, W. Shui, B. L. Carlson, N. Hu, D. Rabuka, J. Lee, C. R. Bertozzi, Site-specific chemical modification of recombinant proteins produced in mammalian cells by using the genetically encoded aldehyde tag. *Proc. Natl. Acad. Sci. U.S.A.* **106**, 3000–3005 (2009). Medline doi:10.1073/pnas.0807820106